

Formation of planetary debris discs around white dwarfs I: Tidal disruption of an extremely eccentric asteroid

Dimitri Veras^{1*}, Zoë M. Leinhardt², Amy Bonsor², Boris T. Gänsicke¹

¹*Department of Physics, University of Warwick, Coventry CV4 7AL, UK*

²*The School of Physics, University of Bristol, Bristol BS8 1TL, UK*

Accepted 2014 September 07. Received 2014 September 07; in original form 2014 June 20

ABSTRACT

25%-50% of all white dwarfs (WDs) host observable and dynamically active remnant planetary systems based on the presence of close-in circumstellar dust and gas and photospheric metal pollution. Currently-accepted theoretical explanations for the origin of this matter include asteroids that survive the star's giant branch evolution at au-scale distances and are subsequently perturbed onto WD-grazing orbits following stellar mass loss. In this work we investigate the tidal disruption of these highly-eccentric ($e > 0.98$) asteroids as they approach and tidally disrupt around the WD. We analytically compute the disruption timescale and compare the result with fully self-consistent numerical simulations of rubble piles by using the N -body code PKDGRAV. We find that this timescale is highly dependent on the orbit's pericentre and largely independent of its semi-major axis. We establish that spherical asteroids readily break up and form *highly eccentric collisionless rings*, which do not accrete onto the WD without additional forces such as radiation or sublimation. This finding highlights the critical importance of such forces in the physics of WD planetary systems.

Key words: minor planets, asteroids: general – stars: white dwarfs – methods: numerical – celestial mechanics – planet and satellites: dynamical evolution and stability – protoplanetary discs

1 INTRODUCTION

The realisation that the rocky material which pollutes white dwarf (WD) atmospheres primarily originates from circumstellar debris and not the interstellar medium (Kilic & Redfield 2007; Gänsicke et al. 2008; Farihi et al. 2009; Jura et al. 2009; Farihi et al. 2010) has revolutionised the study of evolved planetary systems. Precise and extensive observations of metal abundances in WD atmospheres (Zuckerman et al. 2003, 2010; Koester et al. 2014) suggest the presence of dynamically-active systems. This notion is reinforced by secure observations of orbiting dust (Zuckerman & Becklin 1987; Farihi et al. 2012; Xu & Jura 2012) and gas (Gänsicke et al. 2006, 2007, 2008; Debes et al. 2012a).

Whereas the presence of orbiting dust, and its approximate radial distribution, is inferred from measurements of infrared excess luminosity, the existence of gaseous material is instead inferred from metal emission lines, in particular the CaII triplet near 8600 Å. The morphology of the emission line profiles reflect the velocity field of the gas in motion around the WD (see Horne & Marsh 1986), and thereby provide insight into the

spatial distribution of the gas. All of the gaseous system signatures so far discovered constrain the location of the matter to be within or around the WD tidal disruption radius, at about one Solar radius. The two best-studied systems exhibit a noticeable asymmetry in the shape of the double-peaked line profiles, suggesting eccentricities in the range 0.02 to 0.2 (Gänsicke et al. 2006, 2008). In addition, in at least two cases, the shape and strength of the emission lines vary between observations obtained a few years apart, demonstrating evolution of at least the gaseous component of the disc structure on relatively short timescales (Fig. 3 of Gänsicke et al. 2008, Wilson et al. 2014 In Prep).

The complex structure of the gaseous material highlights the dangers of, and simply prove incorrect, assuming all material disrupted around the WD forms a circular disc. What is clear is that for multiple systems, the material is within or around the tidal disruption radius. Hence, these structures cannot have formed during earlier stellar phases, because otherwise they would have resided inside of the progenitor! How they formed during the WD phase remains an outstanding question.

As a first step towards finding an answer, in this work we consider the disruption process of a rubble-pile asteroid around a WD with help from the sophisticated N -body numerical code

* E-mail: d.veras@warwick.ac.uk

Table 1. Timescales used in this paper.

Timescale Symbol	Timescale Name	Equation Number(s)
t_c	Crossing or Disruption	12, 14, 17
P_ω	GR Pericentre Precession	19
t_{fill}	Filling	25
τ_{dyn}	Dynamical	26
τ_{orb}	Orbital	27
τ_{enc}	Encounter	28-29
Δt	Simulation Timestep	31

PKDGRAV (Richardson et al. 2000; Stadel 2001). Although the tidal breakup of rocky asteroidal material has previously been proposed (Graham et al. 1990; Jura 2003; Bear & Soker 2013), the progenitors of these discs could be comets, moons or planets. However, recent theoretical work has favoured asteroids (Bonsor et al. 2011; Debes et al. 2012b; Frewen & Hansen 2014) primarily due to the low frequency of planetary collisions with WDs (Veras et al. 2013; Mustill et al. 2014) and the compositional inconsistencies (Zuckerman et al. 2007) and dynamical difficulties (Stone et al. 2014; Veras et al. 2014a) of comet accretion; investigation of moons is needed. Henceforth we use the term *asteroids* to refer to any small bodies.

In the Solar System, asteroids are known to reside within several tens of au of the Sun. Exo-asteroids at similar separations which survive dynamical instabilities or tidal engulfment during the giant branch phases of their parent stars will harbour wider orbits by a factor of a few, and not be ejected due to mass loss alone (Veras et al. 2011) even for particularly violent stellar structure assumptions (Veras & Wyatt 2012). At a minimum, the asteroids need to reside beyond about a couple of au to avoid engulfment into their star’s giant branch envelope (Mustill & Villaver 2012). Therefore remnant asteroids are expected to reside at distances between a few au and a couple hundred au, and these asteroids can be flung towards the WD only on extremely eccentric orbits. Here we are unconcerned with the dynamical architectures that would be necessary to propel the asteroid to the WD in this manner (see Bonsor et al. 2011; Debes et al. 2012b; Frewen & Hansen 2014) but rather focus entirely on the disruption process.

This paper contains 6 sections, and introduces several timescales, which are summarised in Table 1 for ease of reference. Section 2 establishes the location of the critical disruption sphere and provides a link to the WD radius and mass. Section 3 describes the orbit of an extremely eccentric asteroid with respect to the critical disruption sphere. In Section 4, we analytically determine the timescale for forming an eccentric ring from the disruption. We set up and run our numerical simulations of the disruption in Section 5 before concluding in Section 6.

2 CRITICAL DISRUPTION RADIUS

We define disruption simply as a significant morphological change. Both observations and theory provide strong insight into the critical value at which disruption will occur. Nearly all known planetary rings, which may have been formed from

the disruption of asteroids, are observed to orbit within a few planetary radii from the centre of the planets. The rings around the Centaur Chariklo also lie within a few asteroid radii from the centre of the asteroid (Section 7 of the supplement of Braga-Ribas et al. 2014). Force balance arguments (e.g. pgs. 158-159 of Murray & Dermott 1999) demonstrate that the critical disruption radius r_c has the dependencies given by

$$r_c \propto \left(\frac{M_{\text{WD}}}{M} \right)^{1/3} R, \quad (1)$$

where M_{WD} and M are the masses of the WD and asteroid and R is a fiducial radius of the (not necessarily spherical) asteroid.

The proportionality constant is model-dependent and is based on the shapes, compositions, spin states, orbital states, and criteria used for disruption. The constant may include functions of the tensile or shear strengths of the asteroid (e.g. Davidsson 1999), and may be determined from numerical simulations rather than analytical considerations in order to be liberated from the assumptions of the latter (Richardson et al. 1998). The constant will change depending on whether the asteroid is modelled to simply crack, deform, or dissociate entirely. The disruption radius is famously named after Edouard Roche, although his pioneering calculation was based on just a single set of assumptions.

Because tidal disruption is a dynamic process that in reality cannot be reduced to a simple critical radius criterion, our model makes implicit assumptions. These are that the asteroid is roughly spherical, frictionless and not rotating, or rotating synchronously. These assumptions may both overestimate and underestimate the disruption radius (e.g. Sridhar & Tremaine 1992; Asphaug & Benz 1994, 1996; Bottke et al. 1997; Richardson et al. 1998; Movshovitz et al. 2012). Hence, our proceeding treatment is an oversimplification. However, in order to obtain analytical results, we adopt these assumptions for the remainder of the manuscript.

For our purposes, a useful expression of the disruption radius is

$$\frac{r_c}{R_\odot} = C \left(\frac{M_{\text{WD}}}{0.6M_\odot} \right)^{1/3} \left(\frac{\rho}{3 \text{ g/cm}^3} \right)^{-1/3} \quad (2)$$

where C is a constant ranging from about 0.85 to 1.89 (Bear & Soker 2013), and ρ is the assumed density of the asteroid. The value of $0.6M_\odot$ may be considered as a fiducial WD mass given the mass distribution of all observed WDs (Liebert et al. 2005; Camenzind 2007; Falcon et al. 2010; Tremblay et al. 2013). Due to observational evidence that the vast majority of asteroids have densities which satisfy $\rho \gtrsim 1 \text{ g/cm}^3$ (Table 1 of Carry 2012), we find

$$\max[r_c(M_{\text{WD}})] \equiv r_c^{\text{max}}(M_{\text{WD}}) \approx 2.73 \left(\frac{M_{\text{WD}}}{0.6M_\odot} \right)^{1/3} R_\odot \quad (3)$$

where we have assumed the maximum value of C and minimum value of ρ .

Further, by invoking the Chandrasekhar Limit, which gives the maximum WD mass ($\equiv M_{\text{Ch}} = 1.4M_\odot$), the maximum value of $r_c^{\text{max}}(M_{\text{WD}})$ is $r_c^{\text{max}}(M_{\text{Ch}}) = 3.6R_\odot = 0.017 \text{ au} = 2.5 \times 10^6 \text{ km}$. This value is at least a few hundred times greater than the radius of the WD, which, for a typical WD mass of $0.6M_\odot$, is $\simeq 0.015R_\odot$ (Hamada & Salpeter 1961; Holberg et al. 2012; Parsons et al. 2012). Equation 3 usefully demonstrates just how

small the disruption region is. Any asteroid whose disruption we wish to model must eventually pass inside a sphere with a radius of r_c centred on the WD. Also, because the asteroid might collide with the WD, we must compute R_{WD} .

Both observations and theory demonstrate that mass alone does not uniquely determine the extent of this surface; temperature is another dependence (e.g. Panei et al. 2000). If we neglect this temperature dependence, then equations (27-28) of Nauenberg (1972) link WD mass and radius through the following relation

$$\frac{R_{\text{WD}}}{R_{\odot}} \approx 0.0127 \left(\frac{M_{\text{WD}}}{M_{\odot}} \right)^{-1/3} \sqrt{1 - 0.607 \left(\frac{M_{\text{WD}}}{M_{\odot}} \right)^{4/3}}, \quad (4)$$

where we have assumed a mean molecular weight per electron of 2 (Hamada & Salpeter 1961). Another popular relation is from equation 15 of Verbunt & Rappaport (1988).

$$\frac{R_{\text{WD}}}{R_{\odot}} \approx 0.0114 \sqrt{\left(\frac{M_{\text{WD}}}{1.44M_{\odot}} \right)^{-2/3} - \left(\frac{M_{\text{WD}}}{1.44M_{\odot}} \right)^{2/3}} \times \left[1 + 3.5 \left(\frac{M_{\text{WD}}}{0.00057M_{\odot}} \right)^{-2/3} + \left(\frac{M_{\text{WD}}}{0.00057M_{\odot}} \right)^{-1} \right]^{-2/3}. \quad (5)$$

Both relations produce nearly identical results, with a variation of just a few percent. Further, both relations reproduce well the latest observational results within the error bars (Fig. 4 of Bours et al. 2014).

The higher the WD mass, the smaller the WD radius, so that for $M_{\text{WD}} < M_{\text{Ch}}$, $R_{\text{WD}} > 6.4 \times 10^{-4} R_{\odot} \approx 3.0 \times 10^{-6} \text{au} \approx 445 \text{km}^1$. A small number of WDs with very low masses, down to $0.17M_{\odot}$ (e.g. Brown et al. 2013; Hermes et al. 2013) have been discovered. They are all products of close binary interactions, and it is currently not clear if these systems have any relevance in the context of evolved planetary systems; we no longer consider low mass WDs for the remainder of the paper. For our calculations, we adopt the canonical $0.6M_{\odot}$ mass, which corresponds to a value of $R_{\text{WD}} = 0.0126R_{\odot} \approx 8750 \text{km}$ from equation (4)². Nevertheless, we retain WD mass in all our formulae for future applications. In order to express the critical disruption radius in terms of R_{WD} , we may combine equation (4) with equation (2). Overall, these relations show that disruption predominately occurs at a distance of $\sim 10^5 - 10^6 \text{km}$ ($7 \times 10^{-4} - 7 \times 10^{-3} \text{au}$) from the centre of the WD.

3 ORBIT CHARACTERISTICS

Now that we have quantified the region that asteroids must pass through for disruption to occur, we consider the asteroid orbits themselves. The orbits are noteworthy because of their extreme eccentricity. In fact, any asteroid with a semimajor axis $a > 1 \text{au}$ (like the vast majority of Solar System asteroids) must have an extremely eccentric ($e > 0.983$) orbit in order to achieve a pericentre within the maximum possible disruption

¹ For perspective, this extreme WD would rank 5th in size amongst the Uranian satellites.

² This WD would be just 37 per cent larger in radius than the Earth.

radius [$r_c^{\text{max}}(M_{\text{Ch}})$]. This section will provide detailed characteristics of this orbit, particularly when the asteroid is within the disruption sphere.

3.1 The speed at pericentre

The speed of the asteroid at pericentre, v_q , is remarkably high. If the semimajor axis and pericentre of the asteroid's orbit are denoted by a and q , then

$$v_q \approx 23.1 \frac{\text{km}}{\text{s}} \left(\frac{M_{\text{WD}}}{0.6M_{\odot}} \right)^{1/2} \left(\frac{a}{1 \text{au}} \right)^{-1/2} \left(\frac{1+e}{1-e} \right)^{1/2} \quad (6)$$

$$= 730 \frac{\text{km}}{\text{s}} \left(\frac{M_{\text{WD}}}{0.6M_{\odot}} \right)^{1/2} \left(\frac{q}{0.001 \text{au}} \right)^{-1/2} \sqrt{1+e}. \quad (7)$$

3.2 The range of interesting pericentres

Disruption can occur only when the pericentre is within r_c . This fact, along with our previous findings, allows us to quantify the minimum (q_{min}) and maximum (q_{max}) pericentres we will consider in this paper. Both q_{min} and q_{max} are expressed in terms of radius and mass of the WD through equations (4) and (3), respectively. Consequently,

$$\frac{q_{\text{max}}}{q_{\text{min}}} = \frac{r_c^{\text{max}}(M_{\text{WD}})}{R_{\text{WD}}} \approx 254 \left(\frac{M_{\text{WD}}}{M_{\odot}} \right)^{2/3} \left[1 - 0.607 \left(\frac{M_{\text{WD}}}{M_{\odot}} \right)^{4/3} \right]^{-1/2}, \quad (8)$$

which yields a value of 217 for a WD mass of $0.6M_{\odot}$.

3.3 Entering and exiting disruption sphere

The part of an asteroid's orbit of the greatest interest, and the part which we will model numerically, is the region inside of the disruption sphere. Suppose the given orbit is centred on a Cartesian reference grid such that the star lies at the fixed position $(ae, 0)$. Without loss of generality, assume the asteroid moves counterclockwise. Then the entry and exit points of the disruption sphere along the orbit, assuming the orbit remains static through pericentre passage, are

$$(x_e, y_e) = \left(\frac{a - r_c}{e}, \pm \frac{1}{e} \sqrt{(1 - e^2) [2ar_c - r_c^2 - a^2(1 - e^2)]} \right). \quad (9)$$

The entry and exit distance, r_e , from the star is just $r_e = r_c$, and the speed at these entry and exit points, v_e , is

$$v_e \approx \sqrt{GM_{\text{WD}} \left(\frac{2}{r_e} - \frac{1}{a} \right)} = 23.1 \frac{\text{km}}{\text{s}} \left(\frac{M_{\text{WD}}}{0.6M_{\odot}} \right)^{1/2} \left(\frac{a}{1 \text{au}} \right)^{-1/2} \left(\frac{2+e}{2-e} \right)^{1/2}. \quad (10)$$

Equation (10) should be compared with equation (6). One then observes in the limit of $e \rightarrow 1$, for $e > 0.983$, we obtain

$$\frac{v_e}{v_q} \approx \sqrt{\frac{3}{2}} (1 - e) < 16\% \quad (11)$$

meaning that the pericentre velocity typically exceeds both the entry and exit velocity by about one order of magnitude. This result showcases how drastically the asteroid's velocity changes just within the small disruption sphere even if no disruption occurs.

3.4 Time spent within the disruption sphere

The time spent within the disruption sphere, t_c , will help us predict how the extent of disruption is linked to a particular orbit. We estimate this crossing timescale by assuming the orbit remains static. We obtain

$$t_c = \frac{2|\Pi_e|}{n} \quad (12)$$

where the mean motion, $n \approx \sqrt{GM_{\text{WD}}/a^3}$ (excluding the relatively tiny mass of the asteroid), and the mean anomaly, Π_e , at either the entry or exit point, is given by Kepler's equation ($\Pi_e = E_e - e \sin E_e$). The eccentric anomaly, E_e , at these points is obtained from

$$\cos E_e = \frac{1}{e} \left(1 - \frac{r_c}{a} \right). \quad (13)$$

Knowledge of t_c is particularly important in order to effectively set up numerical simulations.

Because the asteroid must not hit the WD and be within the disruption sphere, we have $R_{\text{WD}} < q < r_c$. The time spent in the disruption sphere is equal to zero for $q = r_c$ and varies as q approaches R_{WD} , when the asteroid would be moving fastest (equation 6). We can compute the maximum time by first rewriting t_c as

$$t_c = 2\sqrt{\frac{a^3}{GM_{\text{WD}}}} \times \left\{ \cos^{-1} \left[\frac{1 - \frac{r_c}{a}}{1 - \frac{q}{a}} \right] - \sqrt{\left(1 - \frac{q}{a} \right)^2 - \left(1 - \frac{r_c}{a} \right)^2} \right\}. \quad (14)$$

Consequently, the value of q which gives the maximum t_c is

$$q' = a \left[1 - \sqrt{1 - \frac{r_c}{a}} \right] \quad (15)$$

and

$$\max(t_c) = t_c(q') = \sin^{-1} \left(\frac{r_c}{a} \right) - \sqrt{\frac{r_c}{a} \left(1 - \frac{r_c}{a} \right)}. \quad (16)$$

Figure 1 quantifies these equations for a fiducial WD with $M_{\text{WD}} = 0.6M_{\odot}$. Note how steeply the time spent in the disruption sphere decreases as a function of q after the maximum value is attained at q' . The plot demonstrates that for a fixed value of q , the time spent in the disruption sphere is nearly independent of a except for $a \ll 0.1$ au. Importantly then, we expect the disruption characteristics to be independent of a for all semimajor axes which could survive engulfment on the giant branch phases of stellar evolution. The value of t_c which satisfies nearly all relevant values of a is

$$\lim_{a \rightarrow \infty} [t_c] = \frac{2\sqrt{2}}{3\sqrt{GM_{\text{WD}}}} \left[\frac{r_c^2 + qr_c - 2q^2}{\sqrt{r_c - q}} \right] \quad (17)$$

with the maximum of these values occurring at

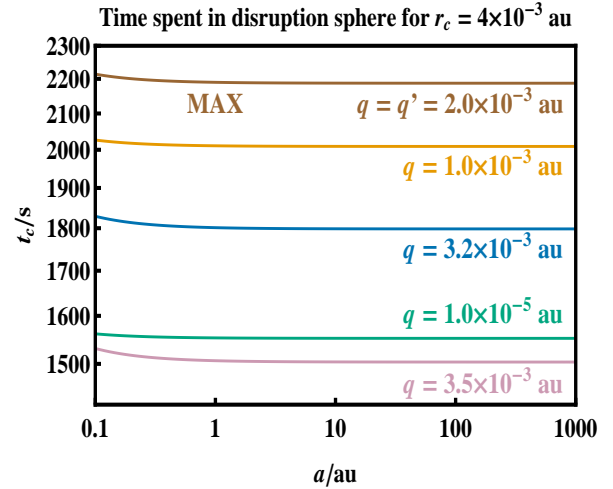


Figure 1. Time an asteroid spends per orbit in a spherical region around a $0.6M_{\odot}$ WD where disruption can occur. The value of t_c is crucially dependent upon the pericentre q but almost independent of the semimajor axis a of the asteroid's orbit. These curves assume a disruption sphere radius of $r_c = 4 \times 10^{-3}$ au. The top curve shows the peak value of the disruption time (equation 18).

$$\lim_{a \rightarrow \infty} [t_c(q')] = \frac{4}{3} \sqrt{\frac{r_c^3}{GM_{\text{WD}}}}, \quad (18)$$

which is a factor of $3/(2\pi)$ times the orbital period of an object that travels along the disruption boundary.

Now we consider the distribution of t_c within the sphere as a function of q . Figure 2 illustrates the result, and that the maximum crossing time does not occur at the WD surface. The reason is because the asteroid is moving the fastest when skimming the surface.

Instead, the maximum disruption or crossing time occurs at $q \approx r_c/2$, which is equivalent to the result of Taylor expanding equation (15) about small values of r_c/a . Note the asymmetry in the curves; the disruption timescale always exceeds 70% of the maximum value unless $q \gtrsim 0.87r_c$. Therefore, as long as the pericentre is not close to the edge of the disruption sphere, the disruption crossing time is approximately constant. In conclusion, the time spent within the disruption radius is typically a few 1000s.

Within the disruption radius, the internal changes the asteroid undergoes are complex and may be strongly dependent on our assumptions of sphericity, frictionlessness and no spin. For example, as observed by Movshovitz et al. (2012), the size distribution of the granular constituents of a real asteroid will affect the relationship between confining pressure and the maximum allowed shear stress. Consequently, disruption may occur within a region other than a sphere, in which case our value of t_c would have to be modified. Further, the shape of the disruption region might change as the asteroid is passing through and changing its own shape and/or spin. Regardless, as illustrated by equation (14) and Figure 1, the total time spent at a pericentre passage is largely independent of the orbit's semimajor axis. This result is independent of the detailed internal dynamical interaction which occurs at the pericentre.

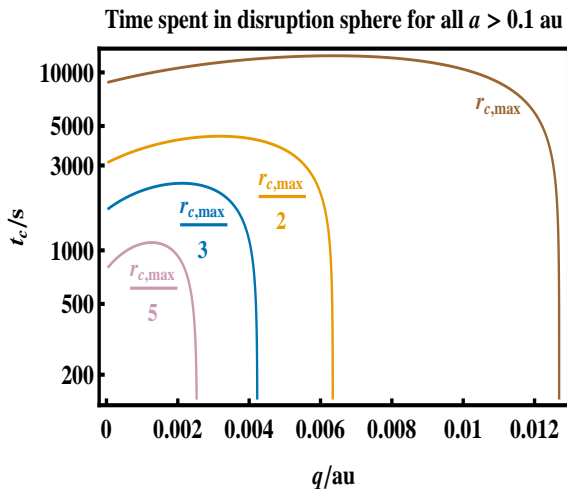


Figure 2. Like Fig. 1, except the crossing time here is plotted as a function of the pericentre q for four different disruption spheres with radii r_c . The maximum possible value of r_c for a $0.6M_\odot$ star is $\max[r_c] \approx 2.73R_\odot$ (0.013 au), and arises from equations (2)-(3), where the unknown parameters are C and ρ . These curves do not visibly change when a is varied beyond about 0.1 au. The peak of each curve occurs approximately halfway between the centre and edge of the sphere, as can be deduced by Taylor expanding equation (15) about small values of r_c/a .

3.5 Contribution from general relativity

As the asteroid approaches the WD, the star will curve space-time, thereby altering the trajectory of the asteroid from the Newtonian value. Here we evaluate this contribution, showing it to be negligible along individual orbits but not necessarily so over secular timescales.

For a single nearly parabolic orbit, Veras (2014) showed that the maximum deviation at the pericentre of a $0.6M_\odot$ star is approximately equal to 2.6 km. When compared with the radius of our adopted WD (8750 km), the extent of the disruption sphere ($10^5 - 10^6$ km), and the error induced by taking the limit of large a in computations (see Fig. 1), this correction is negligible. However, he points out that as q remains fixed as a increases, the approximation get worse, such that for $a = 10^5$ au and $q = 0.1$ au, the error in the estimation is of order unity. Nevertheless, this error is still negligible, and that situation is more relevant for long-period comets than for asteroids.

Over many orbits, general relativity will torque the asteroid's argument (or longitude) of pericentre. This angle will precess over one complete orbit in a time P_ω , where

$$P_\omega \approx 0.15 \text{ Myr} \left[\frac{1 - e^2}{1 - 0.999^2} \right] \left(\frac{M_{\text{WD}}}{0.6M_\odot} \right)^{-3/2} \left(\frac{a}{1 \text{ au}} \right)^{5/2}. \quad (19)$$

Therefore, a precession of a few degrees may occur on thousand-year timescales, which correspond to a few tens of orbits for sufficiently far-away progenitors. Consequently, general relativity would enhance the possibility of collisions amongst debris which is flung out to different semimajor axes. We will consider this possibility, particularly with the disruption of multiple asteroids, in future work.

4 ECCENTRIC RING FORMATION TIMESCALE

Before performing numerical simulations, we can make theoretical predictions about disrupted debris. In particular, we predict that the debris will form an eccentric ring which follows the original orbit. Below we estimate the timescale for formation of this eccentric ring. The extent of the agreement with numerical integrations will help investigators determine the usability of the theoretical model in future studies.

Our treatment follows the formulation presented by Hahn & Rettig (1998), which agreed well with numerical simulations of the disruption of comet Shoemaker-Levy 9. Here, suppose our asteroid is composed of many point mass particles. Later, in our numerical simulations (next section), these particles will adopt nonzero radii. Let all variables with subscript ‘‘P’’ refer to a specific but arbitrary particle. Variables without subscripts refer to the asteroid. In what follows, assume that the breakup is instantaneous and occurs at r_b , and that the particles evolve independently of each other (are *collisionless*) immediately after the breakup. Our formulation is independent of both r_e and r_c .

All particles will move with the same velocity before the asteroid breaks up. Hence,

$$v_P^2 = v^2 = G(M_{\text{WD}} + M) \left(\frac{2}{r_b} - \frac{1}{a} \right). \quad (20)$$

By conservation of energy,

$$-\frac{GM_{\text{WD}}M_P}{2a_P} = \frac{1}{2}M_P v_P^2 - \frac{GM_{\text{WD}}M_P}{r_P} \quad (21)$$

which gives

$$a_P = \frac{ar_b r_P}{\left(\frac{M}{M_{\text{WD}}} \right) r_P (r_b - 2a) + 2a(r_b - r_P) + r_b r_P}. \quad (22)$$

When $r_P = r_b$, that particle continues along the asteroid's original elliptical orbit. When $r_P < r_b$, that particle will have an elliptical orbit. When $r_P > r_b$, that particle can harbour an elliptical, parabolic or hyperbolic orbit. For this last case, consider equation (22). Properties of conic sections dictate that the distance at which the particle's orbit becomes parabolic is

$$r_{\text{crit}} = \frac{2ar_b}{\left(1 + \frac{M}{M_{\text{WD}}} \right) (2a - r_b)} \approx \frac{2ar_b}{2a - r_b} \quad (23)$$

such that the particle's orbit remains elliptical if $r_P < r_{\text{crit}}$ or becomes hyperbolic if $r_P > r_{\text{crit}}$. Note that for asteroids around WDs, we can assume $M/M_{\text{WD}} \approx 0$ because that ratio is about 10 orders of magnitude smaller than any ratio of relevant length scales in this problem.

The velocity gradient between bound debris will fill out a ring. The initial spatial distance between the bound debris will determine the formation timescale. This distance can be up to the entire asteroid diameter, or at minimum the asteroid radius, as all particles between the asteroid centre and the closest point to the WD must remain on bound orbits. The value of r_{crit} determines whether or not all of the particles will remain on bound orbits. Consequently, the debris will fill an entire orbit in a time

$$t_{\text{fill}} = \frac{2\pi}{n(r_P = r_b - R) - n(r_P = r_b + \min(r_{\text{crit}} - r_b, R))}. \quad (24)$$

If t_{fill} is expressed in terms of the asteroid's (original) orbital period (T), then we finally obtain

$$\begin{aligned} \frac{t_{\text{fill}}}{T} &= \frac{n(r_p = r_b)}{n(r_p = r_b - R) - n(r_p = r_b + \min(r_{\text{crit}} - r_b, R))} \\ &= r_b^{\frac{3}{2}} \left[\left\{ \frac{r_b^2 + 2aR - r_b R}{r_b - R} \right\}^{\frac{3}{2}} \right. \\ &\quad \left. - \left\{ \frac{r_b^2 - 2a \times \min(r_{\text{crit}} - r_b, R) + r_b \min(r_{\text{crit}} - r_b, R)}{r_b + \min(r_{\text{crit}} - r_b, R)} \right\}^{\frac{3}{2}} \right]^{-1}. \end{aligned} \quad (25)$$

This formula (equation 25) allow us to generate eccentric disc formation timescales purely analytically. The results are presented in Figs. 3-5 for our fiducial $0.6M_{\text{WD}}$ WD with $r_c = 0.017$ au (see equation 3). Figure 3 illustrates the timescale in terms of years (upper panel) and original orbital periods (lower panel) for five different combinations of the disruption location r_b and the original asteroid radius R as a function of a . The top (blue) curves represent the maximum possible filling time for a 1 km asteroid, which is several orders of magnitude less than a WD cooling time of 1 Gyr. At the other extreme, disruptions where the asteroid skims the WD surface will fill out an eccentric ring with debris in a couple months. Note that the curves in the bottom panel level out beyond a particular semimajor axis value, one that increases with disruption location and decreases with asteroid radius.

Figures 4 and 5 instead highlight the dependence on the disruption distance as a function of both R_{WD} and R , by placing those values on the x -axes. Figure 4 suggests that any asteroids thrown in from an exo-asteroid belt (at ≈ 5 au) or an exo-Kuiper belt (at ≈ 30 au) which reach pericentre values within $10R_{\text{WD}}$ will fill out an eccentric ring within about 100 yrs. Figure 5 further illustrates that the formation timescale is also strongly dependent on the asteroid's radius. Here the x -axis extends to values of 1000 km, which is roughly twice the value of the radius of the largest known asteroid (Ceres) and is comparable to that of small planets³.

As previously mentioned, the results in this section are dependent on the assumption that the breakup is instantaneous and thorough, such that post-breakup, all particles will evolve independently of one another. Our numerical simulations, which are reported in the next section, show that the breakup is never strictly instantaneous. Rather, clumps of particles remain bound for more than one pericentre passage. As the pericentre of the orbit increases, our assumptions break down further, as the clumps become larger and are more strongly bound. Hence, the formulae here are best-suited for close pericentre passages. Further, because our final formula (equation 25) is independent of particle mass or size, the formula should be applicable to asteroids with different particle size distributions as long as the extent of clumping for these rubble piles is negligible. These distributions may be significantly influenced, or even primarily determined,

³ Veras et al. (2013) and Mustill et al. (2014) specifically considered how dynamical instabilities in multi-planet systems may cause a collision with a WD and a planet.

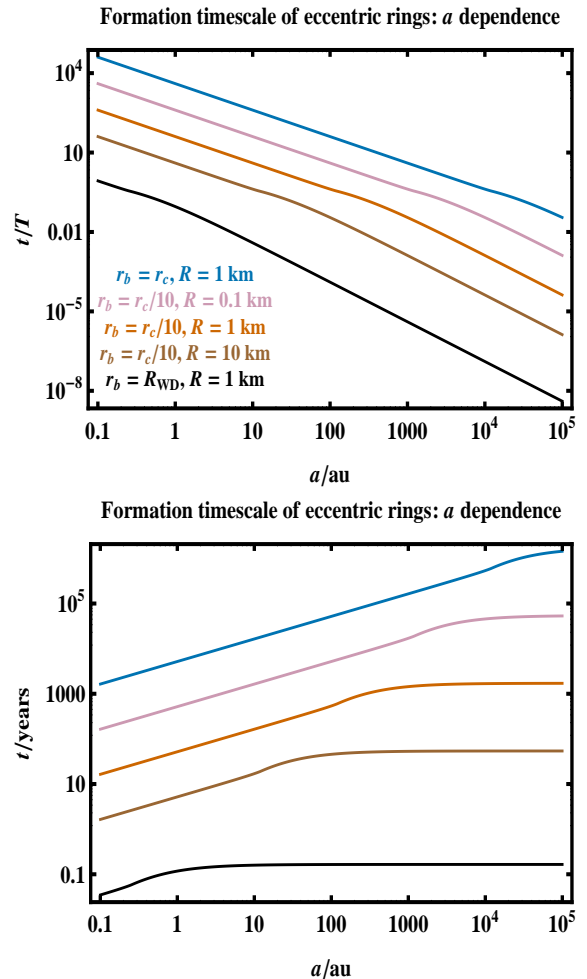


Figure 3. Time which debris takes to fill an eccentric thin ring after an instantaneous disruption of an asteroid at a distance r_b from a WD of mass $0.6M_{\odot}$. The asteroid's original radius and original orbital semimajor axis are R and a , and $r_c = 0.017$ au. The top and bottom panels express filling time in terms of orbital period T and in years, respectively. The plots demonstrate that the formation timescale is highly dependent on r_b , R and a .

by destructive processes occurring during the star's giant branch evolutionary phases (Veras et al. 2014b).

5 NUMERICAL SIMULATIONS

Now we complement our theoretical predictions with numerical simulations of a rubble-pile asteroid. Here we describe the code used, the internal structure of the rubble piles that are modelled, the timestep adopted, and finally our simulation results. Our discussion of the timestep adopted may be widely applicable to other similar N -body codes.

5.1 Numerical disruption code

We use a modified version of the well-established N -body gravity tree code PKDGRAV (Stadel 2001). The major modification is the

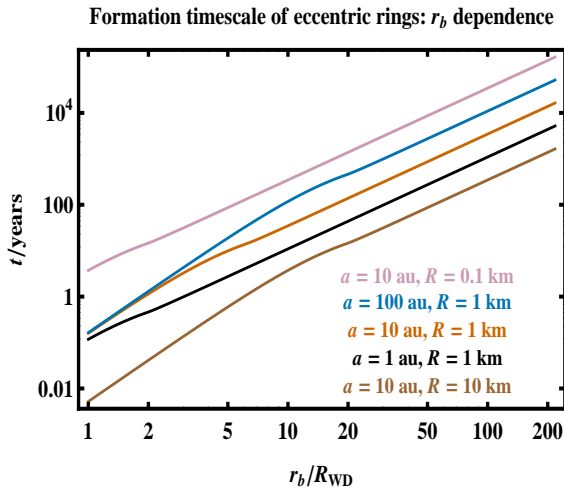


Figure 4. Like Fig. 3, except highlighting the dependence on the disruption distance. For all combinations presented here, when disruption occurs within $10R_{\text{WD}}$, the ring will form within about 100 yrs.

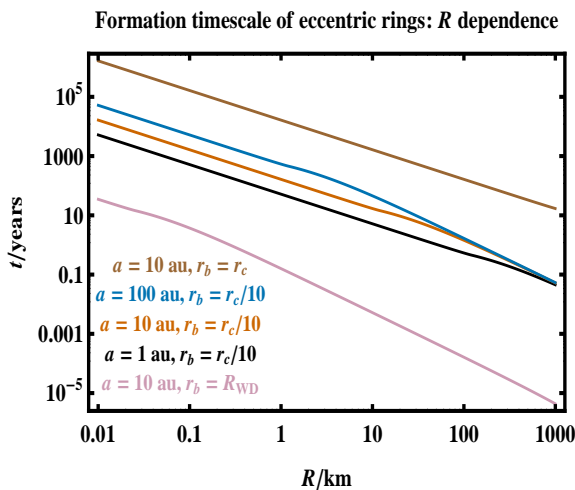


Figure 5. Like Fig. 3, except highlighting the dependence on the radius of the asteroid. The plot shows that any asteroids with $R > 1$ km which skim the WD surface will fill out a ring within a couple months. Also, this plot demonstrates that the filling time has a weak dependence on the semimajor axis of the orbit for constant R .

ability to detect and resolve collisions (Richardson et al. 2000). For our simulations, the N bodies are equal-mass and equal-radius particles which initially comprise a single gravitational aggregate known as a *rubble pile* (although the code is flexible enough to handle interactions between multiple rubble piles; see Leinhardt et al. 2000). As the rubble pile becomes disrupted, the particles’ motion is consistently treated by the code. The WD, or any parent star, may be introduced into the code, but is not treated as one of the N bodies. Instead, the WD is treated as a gravitational point mass (with zero radius). Hence employing a realistic mass-radius relation (equation 4) in the setup is crucial so that orbits do not pass through a region where the WD should reside.

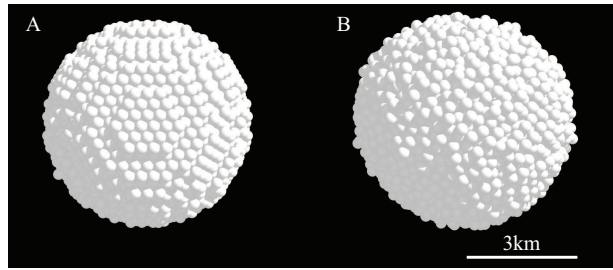


Figure 6. Rubble-pile asteroids, each composed of about 5000 indestructible hard spheres that we denote as *particles*. Asteroid A is hexagonally-packed, and asteroid B is randomly-packed. Disruption is very weakly dependent of the packing method as long as the asteroid is roughly spherical.

The integrator used is a second-order leapfrog integrator, which is symplectic in the absence of collisions. For a more extensive discussion on the properties of this integrator, see Richardson et al. (2000).

5.2 Rubble pile characteristics

The number of particles and their bulk shape might significantly affect the details of disruption (e.g. Richardson et al. 1998). Here we consider only roughly spherical rubble piles of 5000 particles, with two different internal structures. One structure consists of hexagonally-packed particles, and the other randomly-packed particles (see Fig. 6). We find, in concert with previous studies which use PKDGRAV, that our choice of rubble-pile configuration makes no discernibly important difference in the outcome of our simulations. Consequently, we henceforth report results from only our randomly-packed rubble-pile simulations. We adopt an asteroid mass of about 2.26×10^{14} kg. The semi-axes of the rubble pile are about 3.25 km, 3.05 km and 2.99 km, yielding a bulk density of about 1.82 g/cm^3 . The spins of all of the particles are randomly oriented.

5.3 Timesteps

We use a fixed timestep in our simulations. Determining the appropriate value of this timestep is crucial to ensure numerical convergence and accurate results. To guide our intuition for the correct value to adopt, we take note of five applicable timescales. The first is the *dynamical* timescale

$$\tau_{\text{dyn}} \propto \frac{1}{\sqrt{G\rho}}. \quad (26)$$

For asteroids, $\tau_{\text{dyn}} \sim 1$ hour. Previous investigations using PKDGRAV (e.g. Leinhardt & Richardson 2002) demonstrate that adopting a timestep Δt which is about two orders of magnitude smaller than τ_{dyn} ($\Delta t \approx 50$ s) sufficiently resolves the collisions amongst the particles in a rubble pile.

The second timescale is the *orbital* timescale

$$\tau_{\text{orb}} = \frac{2\pi a^{3/2}}{\sqrt{GM_{\text{WD}}}}. \quad (27)$$

The orbital timescale of every known asteroid, comet or planet exceeds 1 hour by several orders of magnitude. Hence, typically, $\tau_{\text{orb}} \gg \tau_{\text{dyn}}$. In symplectic simulations of point mass planets

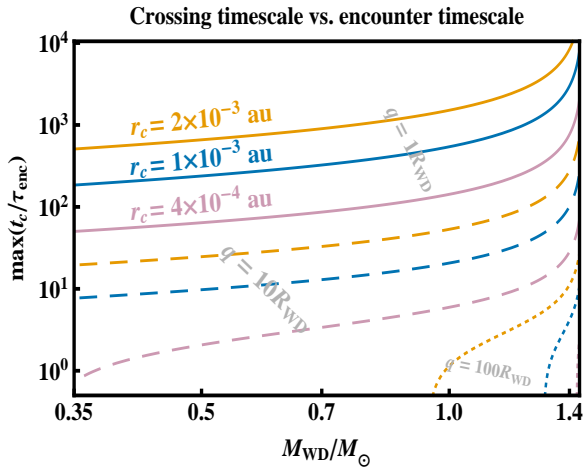


Figure 7. Demonstration that timestep sampling within the disruption sphere is independent of orbital timestep sampling. Ensuring adequate sampling in the former will not guarantee adequate sampling of the latter. The effect is particularly pronounced for pericentres within a few WD radii, and is a strong function of r_c . The solid, dashed and dotted lines refer to $q = 1, 10, 100R_{\text{WD}}$. Visual changes of these curves when sampling different a values greater than 1 au are imperceptible.

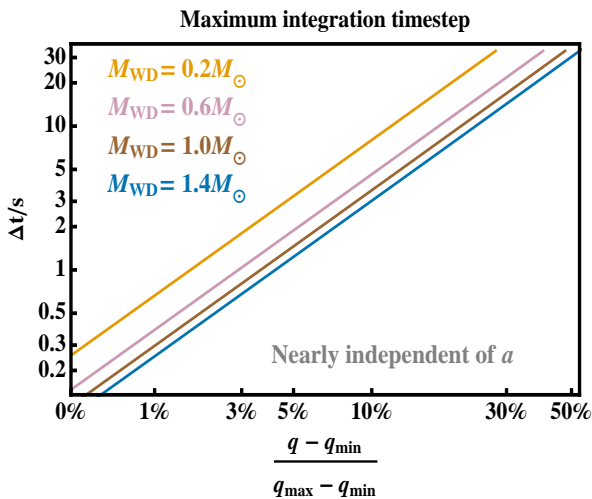


Figure 8. Maximum numerical integration timestep Δt as a function of pericentric distance. Values of q_{min} and q_{max} are given by equation (8). This plot illustrates that for the most relevant disruption region, within the inner half of the disruption sphere, the required timestep is always less than the dynamical timestep of 50 s.

orbiting a star, a well-utilised rule of thumb is $\Delta t \leq (1/20)\tau_{\text{orb}}$ (Duncan et al. 1998).

The third timescale is simply the disruption sphere crossing timescale, t_c . We must ensure that the rubble pile is sufficiently sampled within the disruption sphere. So either the disruption sphere crossing timescale or the dynamical timescale dictates the limiting timestep. However, there is one more consideration.

The fourth timescale is the *encounter* timescale

$$\tau_{\text{enc}} \approx \frac{q}{v_q} = \sqrt{\frac{q^3}{GM_{\text{WD}}}} \left(2 - \frac{q}{a}\right)^{-1/2} \quad (28)$$

$$\approx 205\text{s} \left(\frac{M_{\text{WD}}}{0.6M_{\odot}}\right)^{-1/2} \left(\frac{q}{0.001\text{ au}}\right) \frac{1}{\sqrt{1+e}}, \quad (29)$$

which is the timescale for gravitational interaction at the closest approach distance.

Except near the edge of the disruption sphere, $\tau_{\text{enc}} < t_c$. However, we can obtain a more meaningful comparison by taking the ratio of these two timescales. The value of (t_c/τ_{enc}) is well-approximated at all relevant values of a by

$$\lim_{a \rightarrow \infty} \left(\frac{t_c}{\tau_{\text{enc}}}\right) = \frac{4}{3} \left[\frac{r_c^2 + qr_c - 2q^2}{q^{3/2}\sqrt{r_c - q}}\right] \quad (30)$$

which monotonically decreases as q shifts from R_{WD} to r_c , and hence takes on a maximum value at $q = R_{\text{WD}}$. This ratio is plotted in Fig. 7. The figure demonstrates that the timestep restrictions near the WD surface are demanding. Adopting the dynamical timescale constraint of $\Delta t \approx 50$ s will fail to sufficiently resolve the encounter within a few R_{WD} for the lowest-mass WDs, and within tens of R_{WD} for the highest-mass WDs.

The fifth timescale is the *collision* timescale, τ_{col} , which represents the ratio of a characteristic interparticle distance to the relative velocities of the particles. Because the minimum possible size of a particle orbit is the diameter of the WD, and the particles orbit in the same direction around the WD after disruption, for our purposes $\tau_{\text{col}} > \tau_{\text{dyn}}$ always.

Finally, these considerations lead us to adopt the following timescale for each of our simulations

$$\Delta t = \min\left(50\text{s}, \frac{t_c}{20}, \frac{\tau_{\text{enc}}}{30}\right). \quad (31)$$

The factor of 30 in the last denominator arises from our preliminary simulation suite. We discovered that for higher timesteps, the accumulated error over tens of orbits noticeably alters the argument of pericentre of the orbit.

Because the value of Δt crucially affects the CPU running time of our simulations, we now quantify how Δt varies with a and q . Figure 8 illustrates this dependence, where we have used equations (14) and (28) to compute t_c and τ_{enc} , with r_c given by equation (3). Although its dependence on a is negligible and dependence on M_{WD} is weak, Δt is less than the dynamical timescale of 50s for over half of the distance from q_{min} to q_{max} .

5.4 Simulation results

We seek to answer three important questions from our simulation results: (1) Do rubble piles actually form highly-eccentric rings, as has been theorised? (2) If so, what is the collisional nature of the rings? (3) What is the timescale to fill out the rings with rubble?

5.4.1 Qualitative answers to these questions

Our simulations show that highly-eccentric structures are indeed formed, and are filled-in over time in the rough shape of a ring. Deviations from a perfect filled ring are due to the chaotic nature

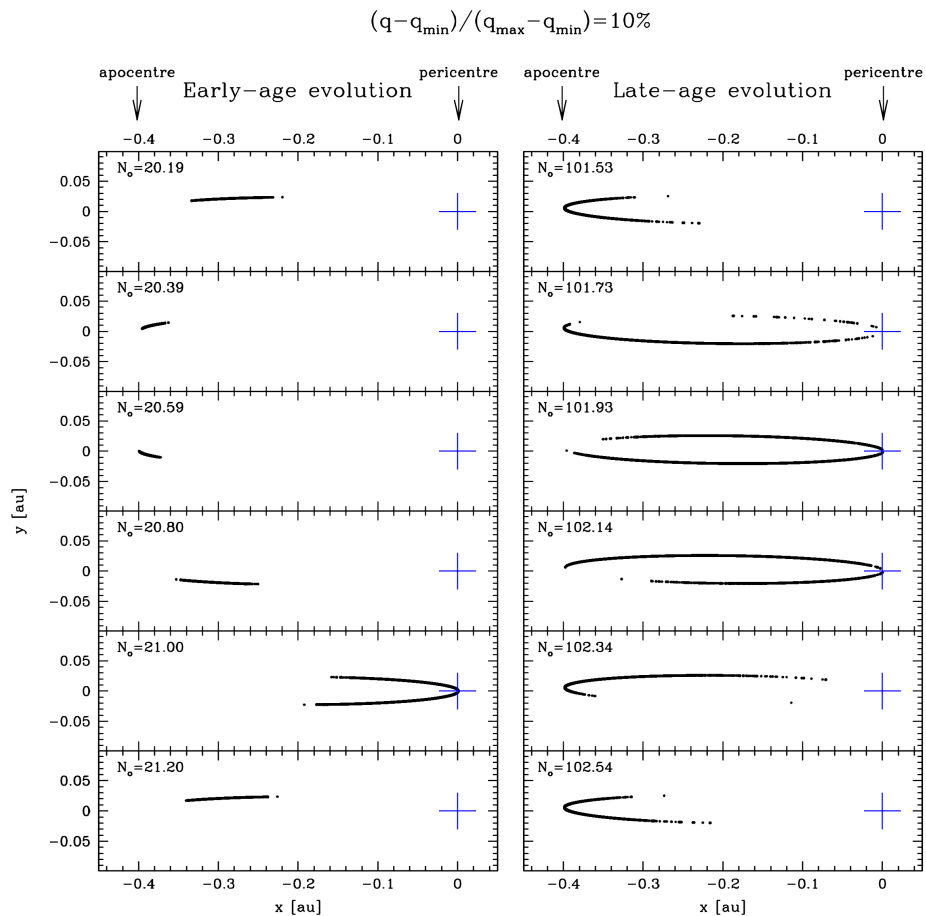


Figure 9. The evolution of a disrupted rubble pile after N_o orbits when $N_o \approx 20$ (left panels) and $N_o \approx 100$ (right panels) from the PKDGRAV numerical code. Snapshots in equal time increments of about 0.202 orbits are displayed from top to bottom. The motion is counterclockwise around the WD, which is denoted with a blue cross and set at the origin. Although the simulations here have $a = 0.2$ au, the qualitative evolution is self-similar for greater orbital distances because the disruption characteristics are largely independent of semimajor axis for $a \gtrsim 0.1$ au. In reality, $a > 1$ au; the value of $a = 0.2$ au was chosen entirely for computational reasons. The plot illustrates the speed at which an eccentric debris ring fills out when the orbital pericentre q satisfies $(q - q_{\min}) / (q_{\max} - q_{\min}) = 10\%$.

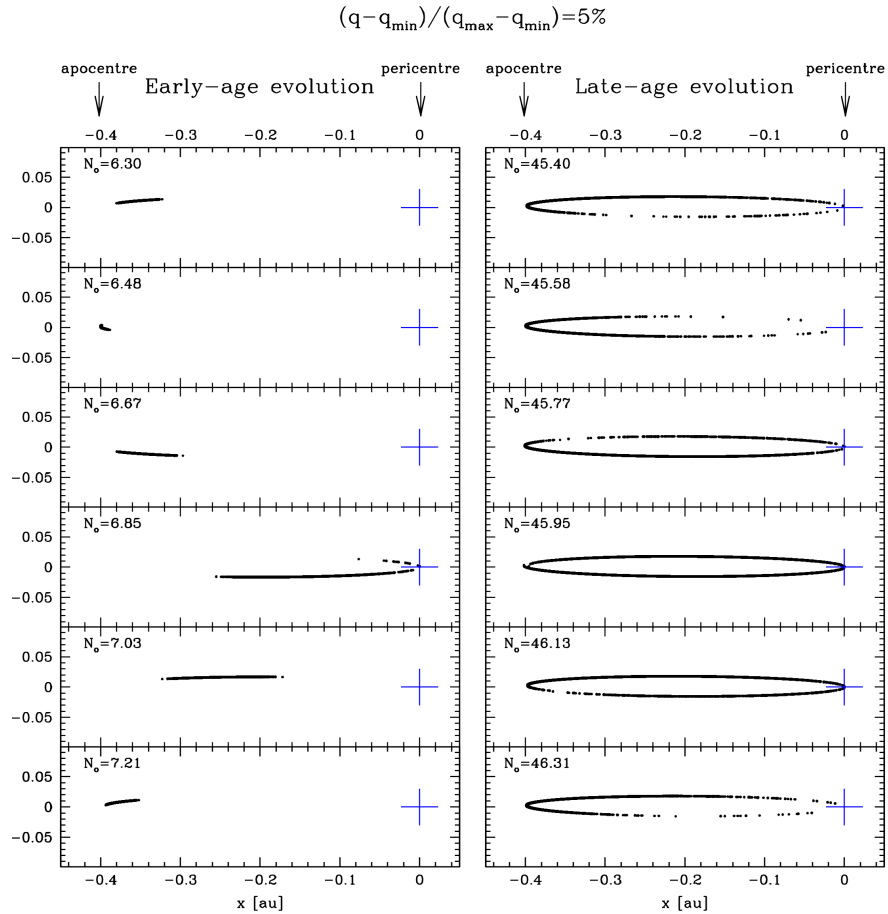


Figure 10. Similar to Fig. 9, except for $(q - q_{\min}) / (q_{\max} - q_{\min}) = 5\%$. Here, the left and right panels show the disrupted rubble pile for $N_o \approx 6$ and $N_o \approx 45$, respectively, demonstrating that the rings fill out more quickly than in Fig. 9. Snapshots in equal time increments of about 0.183 orbits are displayed from top to bottom.

of the non-instantaneous dissociation of thousands of mutually-interacting particles and the amount of material (or number of particles) inside of the asteroid. These deviations take the form of arcs which are void of particles, and brakes in the shape of the annulus itself. The distortion of the shape becomes pronounced only within a few WD radii.

Importantly, our disrupted asteroid eventually completely

dissociates in all cases. Accordingly, each particle eventually orbits the WD without being influenced by any other particle. The result is a *collisionless* collection of particles, each of which propagate according to the classic two-body problem. Gravity alone cannot cause accretion. *They will never accrete onto the WD unless influenced by other forces.* The addition of other forces, such as radiation from the WD and non-gravitational forces from

sublimation, are topics for future work. The timescale at which complete dissociation occurs is a strong function of the initial conditions and particularly the pericentre. Further, complete dissociation is a conservative notion. We have found that well before this condition is satisfied, the particles are effectively collisionless, with just a few 2-particle clumps hanging on for the same amount of time that is taken for the rest of the asteroid to dissociate.

5.4.2 Simulation details

Our simulations were carefully chosen to both showcase important behaviour and finish running on plausible timescales (~ 1 month). The duration of the simulations is severely limited by a timestep which is tiny (see Fig. 8) compared to typical numerical simulations of planetary systems. Consequently, any simulations with semimajor axes of more than a few tenths of an au and a pericentre beyond a few WD radii would require over one month in real time to model a single orbit with PKDGRAV. Fortunately, time spent in the disruption sphere is very weakly dependent on semimajor axis (Fig. 1), allowing us to adopt $a = 0.2$ au and hence model tens of orbits self-consistently with our code. The choice of 0.2 au is motivated only by computational limitations. In reality, no asteroid exist in a WD system on a $a = 0.2$ au orbit. Rather, asteroids should harbour semimajor axes greater, or much greater, than 1 au, but fortunately, the problem scales extremely well for semi-major axes greater than 0.1 au (e.g. Fig. 1).

We display results from two of our simulations in the form of snapshots in Figs. 9-10. These simulations have values of $(q - q_{\min})/(q_{\max} - q_{\min})$ of 10% and 5% respectively. The constant timesteps adopted for the simulations were about 7.356 and 2.772 seconds, respectively, in close accordance with Fig. 8. Hence, the number of steps required to complete one original orbital period were approximately 495,000, and 1,314,000. The original eccentricities of the orbits are about 0.9934 and 0.9966. The simulations assume a WD mass of $0.6M_{\odot}$. The asteroids all begin their motion at $\Pi_0 = -48.96^{\circ}$, a value which affords a “lead-in” time of t_c to the disruption sphere, where t_c is computed according to the orbit which skims the WD.

Figures 9-10 illustrate how disruption typically forms an arc of material which gradually expands into a ring. The expansion is due to the velocity gradient of the particles. These velocities are determined by their last combined interaction with both the WD and another particle just before dissociation from that particle. This process does not reproduce a continuous and uniform velocity distribution because the disruption is not instantaneous. Nevertheless, the approximation used in Section 4 and Figs. 3-5 correspond well with the simulation results: for $a = 0.2$ au, and assuming that the disruption of a roughly 3 km-radius asteroid occurs at the pericentre, the fill-out time is expected to be a few tens to a couple hundred orbits. For semi-major axes of a few au, the fill-out time would then correspond to tens or hundreds of years.

By focusing on the middle of the figures, one can visually discern a slight artificial precession of the ellipse due to accumulated numerical error (despite our conservative timesteps). This precession, which is not due to the general relativistic precession (equation 19) is about twice as prominent in the right column

of Fig. 9 than in Fig. 10 partly due to the former being run for about twice as many orbits.

Finally, in order to test the robustness of our results against the resolution of our rubble piles, we have performed additional simulations with rubble piles which contain nearly 1,000 and 10,000 particles. In each case, we performed simulations with $(q - q_{\min})/(q_{\max} - q_{\min})$ values of 10% and 5%. We find that like in the 5,000-particle case, (1) highly-eccentric collisionless rings are formed, and (2) greater resolution (number of particles) improves the homogeneity of the resulting ring that is formed. More particles help fill in gaps in the ring. We have also repeated our 1,000-particle case using both of the above q values but a different tangential coefficient of restitution (0.5, instead of 1.0). The results were qualitatively similar.

Recent work featuring a higher level of sophistication in the modelling of tidal disruption (e.g. Movshovitz et al. 2012; Yu et al. 2014) showcases potential future directions for follow-up studies. In these cases, particles are idealised not as indestructible hard spheres, but rather as soft spheres (Schwartz, Richardson, & Michel 2012). In the soft sphere discrete element method, rolling and twisting friction may be incorporated between particles, and particles may share multiple points of contact. Particles also need not be modelled as spheres; (Movshovitz et al. 2012) instead use irregular, polyhedral grains.

6 SUMMARY

We have investigated an important step in the process of polluting WDs with circumstellar material: the tidal disruption of bound asteroids which veer into the WD’s Roche radius. We conclude that while an initially spherical asteroid perturbed onto an eccentric orbit may be tidally disrupted by a WD to form a highly eccentric ring of debris, this ring is collisionless without the influences of additional perturbative forces. Without these forces, the disrupted asteroid will not accrete onto the WD, importantly demonstrating that gravity alone is insufficient to produce WD pollution. These results motivate future investigations which would detail how eccentric collisionless rings can form a close-in circumstellar disc (with the approximate dimension of the disruption radius), from where the debris eventually accretes onto the WD.

Although this paper considered the disruption of just a single asteroid, multiple asteroids could arrive at the WD’s disruption radius in quick succession, as the co-orbital fragments of comet Shoemaker-Levy 9 did at Jupiter. Consequently, the filling time for a ring will decrease. The resulting filling timescale depends upon the number of tidally-disrupted asteroids and the relative orientations of the incoming objects, but not their masses (see discussion after equation 25). The masses will determine the extent and number of the gaps in the ring, causing it to appear as a series of loosely- or strongly-connected arcs. If the incoming objects are not initially co-orbital, then they will be disrupted at different pericentres, and instead form a series of rings akin to the ring system of a giant outer Solar system planet. A packed collection of rings may be classified as a disc.

Our more specific findings include a characterisation of the interplay between the extremely eccentric orbits of these asteroids and the WD’s Roche radius (Section 3). Consequently, we

conjecture that the characteristics of disruption is largely independent of semimajor axis (Fig. 1), and highly dependent on the pericentre (Fig. 2 and equation 17). Our work has revealed that the debris follows the original orbit, first as a short arc and then later as a full ring after a time given by equation (25) and Figs. 3-5. Numerical simulations with the rubble-pile integrator PKDGRAV disclose that the debris does not uniformly fill out the ring (Figs. 9-10). To prevent significant artificial precession due to accumulated numerical error, the required maximum timesteps for these types of simulations are extreme, often on the order of one second (equation 31).

ACKNOWLEDGMENTS

We thank the referee for helpful suggestions. We also thank Mia Mace for ray-tracing Fig. 6, and J.J. Hermes, Derek C. Richardson, and Steinn Sigurdsson for useful discussions. The research leading to these results has received funding from the European Research Council under the European Union's Seventh Framework Programme (FP/2007-2013) / ERC Grant Agreement n. 320964 (WDTracer).

REFERENCES

- Asphaug, E., & Benz, W. 1994, *Nature*, 370, 120
 Asphaug, E., & Benz, W. 1996, *Icarus*, 121, 225
 Bear, E., & Soker, N. 2013, *New Astronomy*, 19, 56
 Bochkarev, K. V., & Rafikov, R. R. 2011, *ApJ*, 741, 36
 Bonsor, A., & Wyatt, M. 2010, *MNRAS*, 409, 1631
 Bonsor, A., Mustill, A. J., & Wyatt, M. C. 2011, *MNRAS*, 414, 930
 Bottke, W. F., Richardson, D. C., & Love, S. G. 1997, *Icarus*, 126, 470
 Bours, M. C. P., Marsh, T. R., Parsons, S. G., et al. 2014, *MNRAS*, 438, 3399
 Braga-Ribas, F., Sicardy, B., Ortiz, J. L., et al. 2014, *Nature*, 508, 72
 Brown, W. R., Kilic, M., Allende Prieto, C., Gianninas, A., & Kenyon, S. J. 2013, *ApJ*, 769, 66
 Buonanno, A., Faye, G., & Hinderer, T. 2013, *Physical Review D*, 87, 044009
 Camenzind, M. 2007, *Compact objects in astrophysics : white dwarfs, neutron stars and black holes*, *Astronomy and astrophysics library*. Edited by M. Camenzind. ISBN 9783540257707 Berlin: Springer-Verlag, 2007,
 Carry, B. 2012, *P&SS*, 73, 98
 Carter, B., & Luminet, J.-P. 1983, *A&A*, 121, 97
 Davidsson, B. J. R. 1999, *Icarus*, 142, 525
 Debes, J. H., & Sigurdsson, S. 2002, *ApJ*, 572, 556
 Debes, J. H., Kilic, M., Faedi, F., et al. 2012a, *ApJ*, 754, 59
 Debes, J. H., Walsh, K. J., & Stark, C. 2012b, *ApJ*, 747, 148
 Dong, R., Wang, Y., Lin, D. N. C., & Liu, X.-W. 2010, *ApJ*, 715, 1036
 Duncan, M. J., Levison, H. F., & Lee, M. H. 1998, *AJ*, 116, 2067
 Falcon, R. E., Winget, D. E., Montgomery, M. H., & Williams, K. A. 2010, *ApJ*, 712, 585
 Farihi, J., Jura, M., & Zuckerman, B. 2009, *ApJ*, 694, 805
 Farihi, J., Barstow, M. A., Redfield, S., Dufour, P., & Hambly, N. C. 2010, *MNRAS*, 404, 2123
 Farihi, J., Gänsicke, B. T., Steele, P. R., et al. 2012, *MNRAS*, 421, 1635
 Frewen, S. F. N., & Hansen, B. M. S. 2014, *MNRAS*, 439, 2442
 Gänsicke, B. T., Marsh, T. R., Southworth, J., & Rebassamansergas, A. 2006, *Science*, 314, 1908
 Gänsicke, B. T., Marsh, T. R., & Southworth, J. 2007, *MNRAS*, 380, L35
 Gänsicke, B. T., Koester, D., Marsh, T. R., Rebassamansergas, A., & Southworth, J. 2008, *MNRAS*, 391, L103
 Graham, J. R., Matthews, K., Neugebauer, G., & Soifer, B. T. 1990, *ApJ*, 357, 216
 Hahn, J. M., & Rettig, T. W. 1998, *P&SS*, 46, 1677
 Hamada, T., & Salpeter, E. E. 1961, *ApJ*, 134, 683
 Hermes, J. J., Montgomery, M. H., Gianninas, A., et al. 2013, *MNRAS*, 436, 3573
 Holberg, J. B., Oswalt, T. D., & Barstow, M. A. 2012, *AJ*, 143, 68
 Horne, K., & Marsh, T. R. 1986, *MNRAS*, 218, 761
 Jura, M. 2003, *ApJL*, 584, L91
 Jura, M., Muno, M. P., Farihi, J., & Zuckerman, B. 2009, *ApJ*, 699, 1473
 Kilic, M., & Redfield, S. 2007, *ApJ*, 660, 641
 Kim, S. S., Park, M.-G., & Lee, H. M. 1999, *ApJ*, 519, 647
 Koester, D., Gänsicke, B. T., & Farihi, J. 2014, *A&A*, 566, A34
 Leinhardt, Z. M., Richardson, D. C., & Quinn, T. 2000, *Icarus*, 146, 133
 Leinhardt, Z. M., & Richardson, D. C. 2002, *Icarus*, 159, 306
 Leinhardt, Z. M., Ogilvie, G. I., Latter, H. N., & Kokubo, E. 2012, *MNRAS*, 424, 1419
 Liebert, J., Bergeron, P., & Holberg, J. B. 2005, *ApJS*, 156, 47
 Metzger, B. D., Rafikov, R. R., & Bochkarev, K. V. 2012, *MNRAS*, 423, 505
 Movshovitz, N., Asphaug, E., & Korycansky, D. 2012, *ApJ*, 759, 93
 Murray, C. D., & Dermott, S. F. 1999, *Solar system dynamics by Murray, C. D.*, 1999,
 Mustill, A. J., & Villaver, E. 2012, *ApJ*, 761, 121
 Mustill, A. J., Veras, D., & Villaver, E. 2014, *MNRAS*, 437, 1404
 Nauenberg, M. 1972, *ApJ*, 175, 417
 Panei, J. A., Althaus, L. G., & Benvenuto, O. G. 2000, *A&A*, 353, 970
 Parsons, S. G., Marsh, T. R., Gänsicke, B. T., et al. 2012, *MNRAS*, 420, 3281
 Rafikov, R. R. 2011a, *ApJL*, 732, L3
 Rafikov, R. R. 2011b, *MNRAS*, 416, L55
 Rafikov, R. R., & Garmilla, J. A. 2012, *ApJ*, 760, 123
 Richardson, D. C., Bottke, W. F., & Love, S. G. 1998, *Icarus*, 134, 47
 Richardson, D. C., Quinn, T., Stadel, J., & Lake, G. 2000, *Icarus*, 143, 45
 Schwartz, S. R., Richardson, D. C., & Michel, P. 2012, *Granular Matter*, 14, 363
 Sridhar, S., & Tremaine, S. 1992, *Icarus*, 95, 86
 Stadel, J. G. 2001, Ph.D. Thesis,
 Stone, N., Sari, R., & Loeb, A. 2013, *MNRAS*, 435, 1809
 Stone, N., Metzger, B., & Loeb, A. 2014, arXiv:1404.3213

- Tremblay, P.-E., Ludwig, H.-G., Steffen, M., & Freytag, B. 2013, *A&A*, 559, A104
- Veras, D., Wyatt, M. C., Mustill, A. J., Bonsor, A., & Eldridge, J. J. 2011, *MNRAS*, 417, 2104
- Veras, D., & Wyatt, M. C. 2012, *MNRAS*, 421, 2969
- Veras, D., Mustill, A. J., Bonsor, A., & Wyatt, M. C. 2013, *MNRAS*, 431, 1686
- Veras, D. 2014, *MNRAS*, 442, L71
- Veras, D., Shannon, A., Gänsicke, B. T., 2014a, Submitted to *MNRAS*
- Veras, D., Jacobson, S.A., Gänsicke, B. T., 2014b, Submitted to *MNRAS*
- Verbunt, F., & Rappaport, S. 1988, *ApJ*, 332, 193
- Voyatzis, G., Hadjidemetriou, J. D., Veras, D., & Varvoglis, H. 2013, *MNRAS*, 430, 3383
- Xu, S., & Jura, M. 2012, *ApJ*, 745, 88
- Yu, Y., Richardson, D. C., Michel, P., Schwartz, S. R., & Baloulou, R.-L. 2014, arXiv:1408.0168
- Zuckerman, B., Koester, D., Reid, I. N., Hüensch, M. 2003, *ApJ*, 596, 477
- Zuckerman, B., Koester, D., Melis, C., Hansen, B. M., & Jura, M. 2007, *ApJ*, 671, 872
- Zuckerman, B., Melis, C., Klein, B., Koester, D., & Jura, M. 2010, *ApJ*, 722, 725
- Zuckerman, B., & Becklin, E. E. 1987, *Nature*, 330, 138